11th International Symposium on Turbulence and Shear Flow Phenomena (TSFP11)
Southampton, UK, July 30 to August 2, 2019

REYNOLDS NUMBER EFFECTS ON SWIRLING PIPE FLOWS

R. C. Chin
School of Mechanical Engineering
The University of Adelaide
The University of Adelaide, SA - 5005, Australia
rey.chin@adelaide.edu.au

J. Philip
Department of Mechanical Engineering
The University of Melbourne
The University of Melbourne, VIC - 3010, Australia
jimmyp@unimelb.edu.au

ABSTRACT

Direct numerical simulation of a swirling pipe flow is performed to investigate the effects of Reynolds number and swirl on turbulence statistics. The swirling motion is imposed via a constant azimuthal body force coupled with a body force in the axial direction that drives the flow. The friction Reynolds numbers are $Re_\tau \approx 170$ and 500 with a pipe length of $8\pi\delta$ (where δ is the pipe radius). The simulations are performed with a swirling force matching that of the axial forcing. The swirling motion appears to have an opposite influence on the near-wall axial flow statistics for the two Reynolds numbers. An analysis of the azimuthal turbulence statistics lead to an introduction of a mixed scaling to collapse the azimuthal velocity profiles and the total stresses.

Introduction

Swirling flow in a confined region has many engineering applications, and we are motivated by two specific scenarios: (i) combustion chambers — where the incoming flow is swirled to stabilise the flame, and (ii) transport and separation in particle laden flows — where swirling flow in a pipe can centrifugally separate the particles due to their higher density compared to the fluid.

Typically the effect of swirl on turbulent pipe flow is studied by either rotating the pipe walls which has the usual axial flow – where the maximum axial velocity is at the wall and called a *centripetal* swirl (Orlandi & Fatica, 1997; Eggels, 1994; Leclaire & Jacquin, 2012; Facciolo *et al.*, 2007)), or by imposing an azimuthal flow over the existing axial flow – where the maximum axial velocity is somewhere between the wall and the centerline, and called a *centrifugal* swirl (Kitoh, 1991; Pierce & Moin, 1998; Zonta & Soldati, 2013). The latter method is more practical in industrial scenarios where azimuthal jets of air are injected into an axial pipe flow. Although numerically this can be simulated where the flow develops downstream, however, if the flow development (after a short transient) is happening slowly, one can use an axially periodic computational domain and implement efficient simulation strategies by using an azimuthal body force. Pierce & Moin (1998) studied several body force implementation strategies, and we follow a similar method (to be explained in detail later). We note here that most studies (computationally as well as in laboratory experiments) have considered the case of a rotating pipe wall, which is relatively 'simple' to understand.

Aims:
As such, we observe that there is a dearth of data for centrifugal swirl cases, and one of the aims of this paper is to present direct numerical simulation (DNS) data for different axial Reynolds number (Re_τ) and swirl strengths. This extends our earlier work (Chin & Philip, 2018) where we looked at a fixed Re_τ. Here, $Re_\tau = u_{\tau,x}\delta/\nu$, where $u_{\tau,x}$ is the x-direction friction velocity $= \sqrt{\nu\, \mathrm{d}U_x/\mathrm{d}y|_{y=0}}$ with $y := \delta - r$, δ the pipe radius and ν the kinematic viscosity of the fluid. We take $(x,\ r,\ \theta)$ coordinate system with $(U_x,\ 0,\ U_\theta)$ and $(u_x,\ u_r,\ u_\theta)$ the corresponding mean and fluctuating velocities, respectively. Secondly, we want to test the scaling of basic turbulent statistics, such as, mean axial and azimuthal velocities as well as the turbulent stresses. In an axial flow with no swirl, the $u_{\tau,x}$ is the typical scaling velocity close to the wall, where as in swirling flows we now have $u_{\tau,\theta} = \sqrt{\nu\, \mathrm{d}U_\theta/\mathrm{d}y|_{y=0}}$, and the appropriate scaling velocity for different turbulent statistics is unclear.

Swirl generation and the numerical method

As briefly mentioned above, we intend to simulate a scenario wherein once the swirling flow enters the pipe, it is in an 'equilibrium' condition, i.e., the swirl strength is constant and does not decay downstream. This is a reasonable assumption if we consider a section of the pipe that is short compared to the distance over which swirl decays. The axially and azimuthally averaged mean axial and azimuthal

momentum equations are (e.g., Pierce & Moin, 1998):

$$\frac{1}{r}\frac{\mathrm{d}}{\mathrm{d}r}(r\tau_{xr}) + f_x = 0, \tag{1a}$$

$$\frac{1}{r}\frac{\mathrm{d}}{\mathrm{d}r}(r\tau_{r\theta}) + \frac{\tau_{r\theta}}{r} + f_\theta = 0, \tag{1b}$$

where, the total stresses (per unit density) $\tau_{xr} = \nu\frac{\mathrm{d}U_x}{\mathrm{d}r} - \langle u_r u_x\rangle$, and $\tau_{r\theta} = \nu\left(\frac{\mathrm{d}U_\theta}{\mathrm{d}r} - \frac{U_\theta}{r}\right) - \langle u_r u_\theta\rangle$. Here, f_x is the forcing in x equal to the constant axial pressure gradient (per unit density), and f_θ is the azimuthal forcing, given by $f_\theta = af_x$, whereby a is a percentage of f_x.

Pierce & Moin (1998) have compared different kinds of forcing, $f_\theta(r)$, and don't find significant differences between them. Our choice is based on simplicity in implementation and also the resultant mean equations of motion in (1). The swirl number S is the ratio of the axial fluxes of the azimuthal to axial momentum defined as,

$$S = \frac{\int \rho U_x U_\theta r^2 \,\mathrm{d}r\mathrm{d}\theta}{\delta \int \rho U_x^2 \, r \,\mathrm{d}r\mathrm{d}\theta}. \tag{2}$$

To perform the swirling pipe flow simulations, fully developed turbulent pipe flow data from Chin *et al.* (2010) is utilised to start the simulation. The numerical scheme employed to perform the pipe flow simulations is detailed in Blackburn & Sherwin (2004). The fluid flow in the axial and azimuthal directions is driven by the body forces f_x and f_θ, respectively. The f_x utilised in the simulations correspond to friction Reynolds numbers of $Re_\tau \approx 170$ and 500. The simulations parameters are summarised in table 1.

Results

Here we present four different simulations, corresponding to $a = 0\%$ (no forcing, **L0**) and 100% (**L100**) forcing at the lower Reynolds number $Re_\tau \approx 170$; no forcing (**H0**) and 100% (**H100**) at moderate Reynolds number $Re_\tau \approx 500$. Figure 1 shows the contours of the instantaneous axial velocity $\tilde{u_x}$ close to the wall at $y^+ \approx 15$ for the four cases. The near wall streaks with the azimuthal spacing of ≈ 100 viscous units are present in figure 1(a) for no forcing. With forcing, in figure 1(b), the streaks tilt at an angle due to the azimuthal mean velocity. Interestingly, we observe a more organised patch of streaks with imposed swirl, as if the low momentum regions are trying to separate from the high momentum ones. With increasing Re_τ (c.f., figure 1c), the streaks are still of the same size ≈ 100 viscous units, although now they appear smaller due to the figure scaled in outer units. We note that with similar percentage of azimuthal forcing, the $Re_\tau \approx 500$ case exhibits higher axial velocity than the $Re_\tau \approx 170$ case. With swirl (c.f., figure 1d), we now observe a more organised low and high momentum regions, again tilted due to the non-zero U_θ. These organised banded motion is reminiscent of the laminar-turbulent patterns in transitional shear flows (e.g., Prigent *et al.*, 2002; Duguet *et al.*, 2010; Philip & Manneville, 2011; Chantry *et al.*, 2016). Although the Reynolds numbers are far off from the transitional regime, we speculate that the swirl has a tendency to make the flow less turbulent (especially close to the wall), and any process that tries to reduce the turbulence levels forces the flow to organise spatially into low/high turbulence regions. The organisation we see in figure 1(d) could have some links to this patterning mechanism.

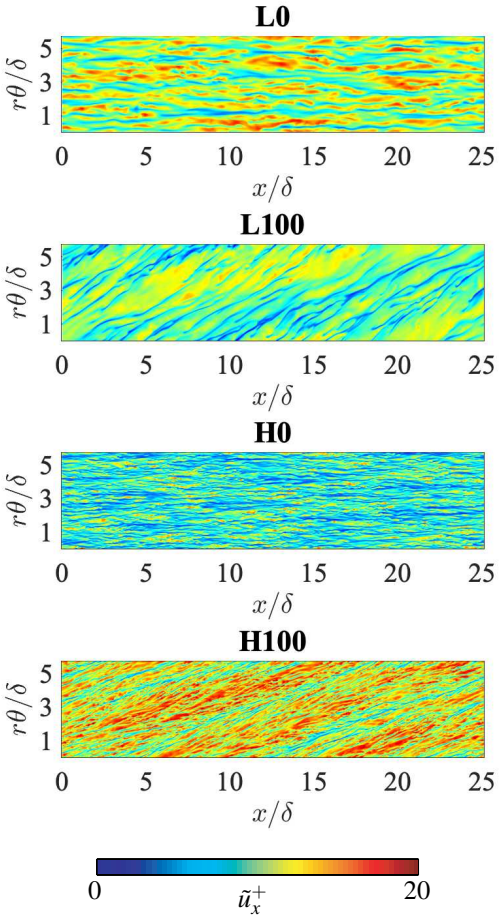

Figure 1. Instantaneous axial vorticity in the $x-r\theta$ plane for all cases at wall-normal location $y^+ \approx 15$. From top to bottom: low Reynolds number non-swirling pipe **L0**, low Reynolds number 100% forcing **L100**, moderate Reynolds number non-swirling pipe **H0**, moderate Reynolds number 100% forcing **H100**.

Mean velocity

The mean axial velocity profiles (U_x) are presented in two different ways in figure 2. Here, the black (dark) lines are at low Reynolds numbers ($Re_\tau \approx 170$); solid lines denotes **L0** and dashed lines represent **L100**. The higher Reynolds number cases ($Re_\tau \approx 500$) are in red (lighter) coloured lines, wherein again solid and dashed-lines represent no swirl **H0** and swirl cases **H100**, respectively. Same line-styles are used in subsequent figures too.

Figure 2(a) shows the axial velocity profiles normalised by the bulk velocity of the non-swirling pipe flow. We normalise such that the non-swirl bulk flow $U_{bulk} = 1$. Low Reynolds number shows swirl decreases velocity from the wall to the centre compared to the non-swirl case, whereas for the higher Reynolds number case there is an increased velocity in the near-wall and a decrease in the outer region. This non-monotonic behaviour of swirl with the change in Re_τ suggests that different wall-normal regions of the flow responds slightly differently to swirl, and further investigation focusing on different regions might be

Table 1. Summary of numerical simulation parameters.

Case	Re_τ	f_θ	L_x	Δx^+	Δr^+	$\Delta r\theta^+$	S
L0	170	$0f_x$	$8\pi\delta$	6.7	[0.5, 3.6]	8.4	0
L100	170	$1f_x$	$8\pi\delta$	6.7	[0.5, 3.6]	8.4	0.28
H0	500	$0f_x$	$8\pi\delta$	6.8	[0.07, 5.5]	8.2	0
H100	500	$1f_x$	$8\pi\delta$	6.8	[0.07, 5.5]	8.2	0.17

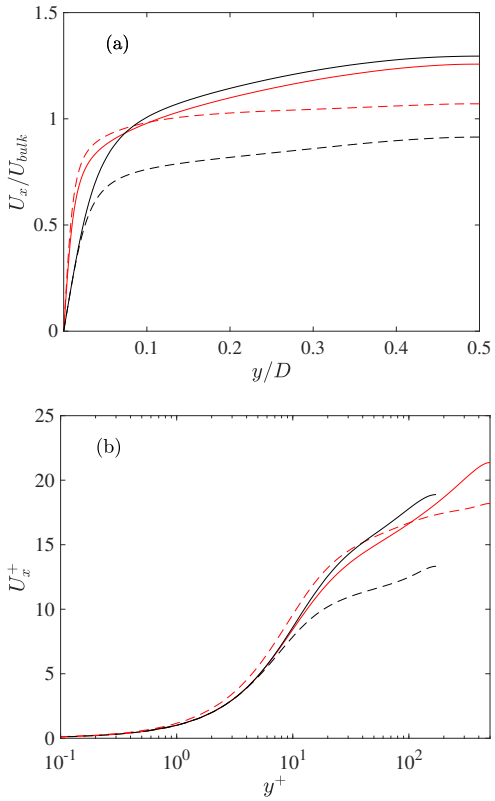

Figure 2. Mean axial velocity profile for all cases. (a) U_x/U_{bulk} versus y/D and (b) U_x normalised by $u_{\tau,x}$ versus y^+. black solid line (**L0**), black dashed-line (**L100**), red solid line (**H0**) and red dashed-line (**H100**).

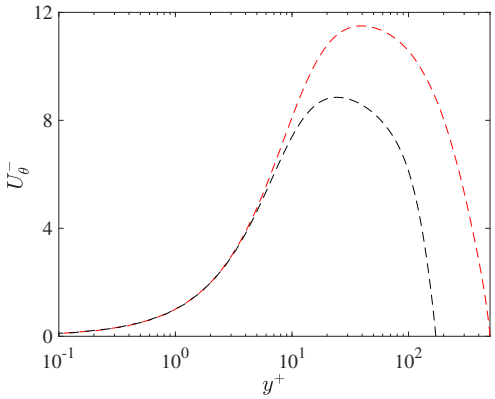

Figure 3. Azimuthal velocity profile for cases **L100** (blue dash-line) and **H100** (blue solid line).

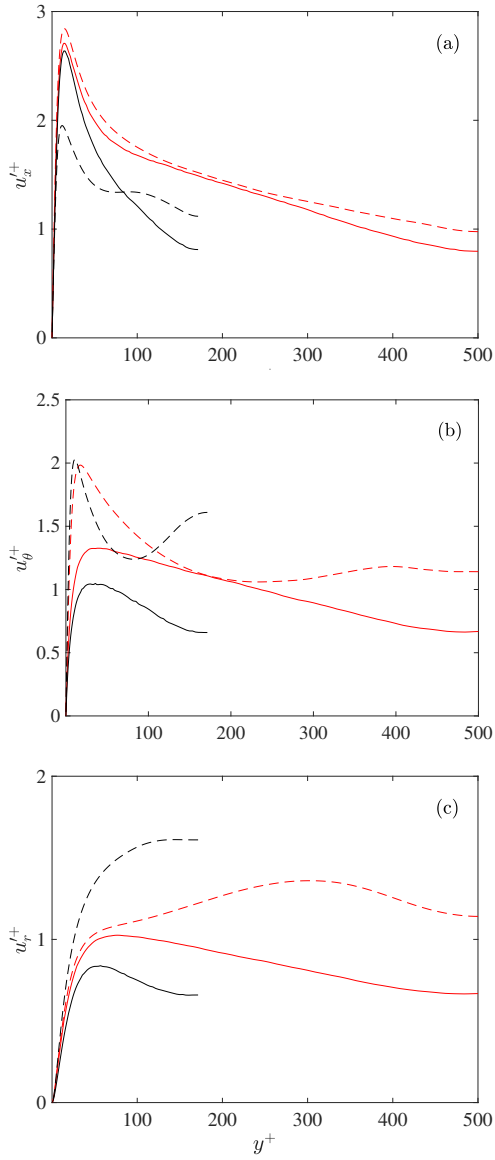

Figure 4. Turbulence intensities of swirling pipe flow compared to DNS straight pipe. (a) Axial velocity turbulence intensity, (b) azimuthal velocity turbulence intensity and (c) radial velocity turbulence intensity. The lines symbols are as in figure 2.

helpful. In figure 2(b) we normalise the mean profile by $u_{\tau,x}$. There is a collapse for low Reynolds number only, and that too close is to the wall. In both Re_τ-cases, it seems that the wake is significantly affected than the near wall-region (except, of course, the mean flow inclination).

The azimuthal mean velocity profiles (U_θ) are presented in figure 3. Again, black dash-line shows the low

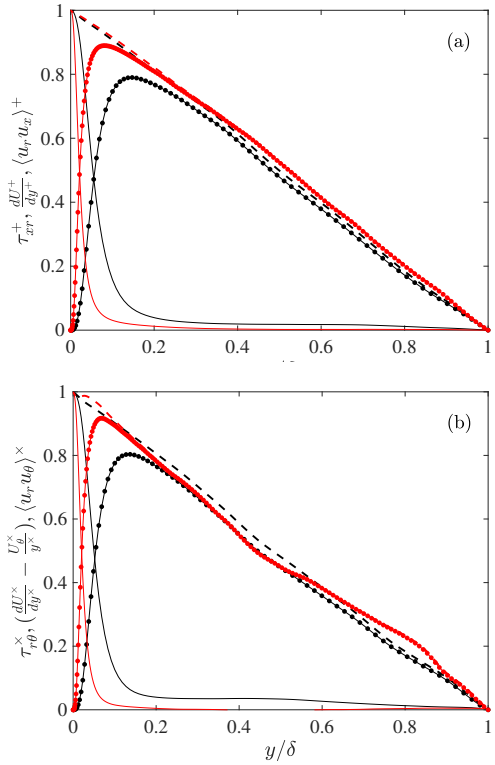

Figure 5. The total stresses Reynolds stress for cases **L100** (black) and **H100** (red). (a) $\tau^+_{xr} = \frac{dU^+_x}{dy^+} - \langle u_r u_x\rangle^+$, dashed lines – τ^+_{xr}, dot line – $\langle u_r u_x\rangle^+$ and solid line – $\frac{dU^+_x}{dy^+}$. (b) $\tau^\times_{r\theta} = \left(\frac{dU^\times_\theta}{dy^\times} - \frac{U^\times_\theta}{y^\times}\right) - \langle u_r u_\theta\rangle^\times$, dashed lines – $\tau^\times_{r\theta}$, dot line – $\langle u_r u_\theta\rangle^\times$ and solid line – $\left(\frac{dU^\times_\theta}{dy^\times} - \frac{U^\times_\theta}{y^\times}\right)$.

Reynolds number case **L100** and red dashed-line is for the moderate Reynolds number case **H100**. Although not shown here, we find that U_θ does not scale well with either $u_{\tau,x}$ or $u_{\tau,\theta}$. Interestingly, a mixed scaling seems to collapse the profile well. The mixed velocity scale $u_{\tau,x\theta} := \mathrm{d}U_\theta/\mathrm{d}y^+ = u_{\tau,\theta}\left(\frac{u_{\tau,\theta}}{u_{\tau,x}}\right)$. We define the normalised U_θ, $U^-_\theta := U_\theta/u_{\tau,x\theta}$. In any case, as expected, the outer region flow (which does not scale with inner variables) increases with increased Reynolds number.

Turbulent normal stresses

The r.m.s for axial, azimuthal and radial velocities, normalised with their corresponding $u_{\tau,x}$, are shown in figure 4(a, b, c) respectively. Figure 4(a) shows a reduced turbulence intensity at the near-wall for low Reynolds number, but an opposite trend is present for higher Reynolds number. In the outer region, both show an increased turbulence intensity for the swirling flows. In the inner region, the trend for higher and lower Re_τ cases are different. This behaviour is similar to what we found for the mean axial velocities. The r.m.s for azimuthal and radial velocities (c.f., figures 4b and c) for the swirling cases show an increase everywhere in the pipe compared its non-swirling counterpart.

Turbulent and total shear stresses

Next we investigate the total shear stresses associated with the mean axial and azimuthal equations of motion. Figure 5(a) shows the axial total stresses for the both low **L100** (black) and high **H100** (red) Reynolds number swirl cases. The total stresses collapse on to the line $\tau^+_{xr} = 1 - y/\delta$, which is similar to a non-swirl pipe flow. This is evident after integrating (1)(a) once. As in the non-swirl case, in the outer region where the viscous component (in solid lines) is small, the turbulent shear stress (in dot-solid lines) follow the $1 - y/\delta$ line. With increasing Reynolds number, the turbulent stress contribution increases while the viscous stress decreases.

The shear stress in the azimuthal direction is presented in figure 5(b). The profiles are normalised by the azimuthal friction velocity $u_{\tau,\theta}$, denoted by a superscript '$\times$'. Since $\tau_{r,\theta}$ is less common than $\tau_{x,r}$, in the following we provide some additional details. Starting with (1b), i.e.,

$$\begin{aligned} \frac{1}{r}\frac{\mathrm{d}}{\mathrm{d}r}(r\tau_{r\theta}) + \frac{\tau_{r\theta}}{r} &= -f_\theta, \quad \text{or,} \\ \frac{\mathrm{d}\tau_{r\theta}}{\mathrm{d}r} + 2\frac{\tau_{r\theta}}{r} &= -f_\theta, \quad \text{and, integrating once,} \\ \tau_{r\theta} = &= -\frac{r}{3}f_\theta + \frac{C}{r^2}, \end{aligned} \tag{3}$$

where C is the contant of integration. Now, applying boundary condition at $r = 0$, implies that $C = 0$. At $r = \delta$, and recalling that $\tau_{r\theta} = \nu\left(\frac{dU_\theta}{dr} - \frac{U_\theta}{r}\right) - \langle u_r u_\theta\rangle$, we obtain,

$$u^2_{\tau,\theta} = -\nu\frac{\mathrm{d}U_\theta}{\mathrm{d}r}\bigg|_{r=\delta} = \frac{\delta}{3}f_\theta. \tag{4}$$

Also, for large r where viscous component of the stress becomes small, and hence (3) reduces to,

$$\begin{aligned} \langle u_r u_\theta\rangle &\approx \frac{r}{3}f_\theta = \frac{(\delta - y)}{3}f_\theta, \quad \text{or,} \\ \langle u_r u_\theta\rangle^\times &\approx 1 - \frac{y}{\delta}, \end{aligned} \tag{5}$$

Figure 5(b) clearly shows this expected trend in $\langle u_r u_\theta\rangle^\times$. Trends similar to τ_{xr} is observed for $\tau_{r\theta}$, where Reynolds stress increases and viscous stress decreases with increasing Reynolds number.

Conclusions

Swirling pipe flows are compared to non-swirling pipe flows at low and moderate Reynolds numbers. When swirl is introduced, we observe a strong tendency for the flow to organise itself into high and low momentum zones in the near-wall region. There is also an increased turbulence intensity associated with the swirling cases. A mixed-scaling is used to collapse the azimuthal velocity profile in the near-wall region. The axial and azimuthal total stresses collapse when scaled with the axial and azimuthal friction velocities respectively. Consistent with the mean equations of motion, both exhibit a slope of -1 in the outer region.

REFERENCES

Blackburn, H. M & Sherwin, J. S. 2004 Formulation of a Galerkin spectral element-Fourier method for three-dimensional incompressible flows in cylindrical geometries. *J Comp. Phys.* **197**, 759 – 778.

Chantry, M., Tuckerman, L. S & Barkley, D. 2016 Turbulent–laminar patterns in shear flows without walls. *J. Fluid Mech.* **791**.

Chin, C., Ooi, A., Marusic, I. & Blackburn, H. M. 2010 The influence of pipe length on turbulence statistics computed from direct numerical simulation data. *Phys. Fluids* **22(11)**, 115107.

Chin, C. R & Philip, J. 2018 Low reynolds number turbulent swirling pipe flows. In *Proceedings of the 21st Australasian Fluid Mechanics Conference, AFMC 2018*. Adelaide, Australia, Australian fluid mechanics society.

Duguet, Y., Schlatter, P. & Henningson, D. S 2010 Formation of turbulent patterns near the onset of transition in plane couette flow. *J. Fluid Mech.* **650**, 119–129.

Eggels, J.G.M. 1994 Direct and large eddy simulation of turbulent flow in a cylindrical pipe geometry. PhD thesis, Delft University of Technologye, Delft University Press.

Facciolo, L., Tillmark, N., Talamelli, A. & Alfredsson, P. H. 2007 A study of swirling turbulent pipe and jet flows. *Phys. Fluids* **19(3)**, 035105.

Kitoh, O. 1991 Experimental study of turbulent swirling flow in a straight pipe. *J Fluid Mech* **225**, 445–479.

Leclaire, B. & Jacquin, L. 2012 On the generation of swirling jets: high-reynolds-number rotating flow in a pipe with a final contraction. *J Fluid Mech* **692**, 78–111.

Orlandi, P. & Fatica, M. 1997 Direct simulations of turbulent flow in a pipe rotating about its axis. *J Fluid Mech* **343**, 43–72.

Philip, J. & Manneville, P. 2011 From temporal to spatiotemporal dynamics in transitional plane couette flow. *Phys. Rev. E* **83** (3), 036308.

Pierce, C. D. & Moin, P. 1998 Method for generating equilibrium swirling inflow conditions. *AIAA* **36(7)**, 1325–1327.

Prigent, A., Grégoire, G., Chaté, H., Dauchot, O. & van Saarloos, W. 2002 Large-scale finite-wavelength modulation within turbulent shear flows. *Phys. Rev. Lett.* **89** (1), 014501.

Zonta, F., Marchioli C. & Soldati, A. 2013 article and droplet deposition in turbulent swirled pipe flow. *Int. J. Multiph. Flow* **343**, 172–183.